Flexural cracking-induced acoustic emission peak frequency shift in railway prestressed concrete sleepers

Janeliukstis, Rims; Clark, Andrew; Papaelias, Mayorkinos; Kaewunruen, Sakdirat

DOI:
10.1016/j.engstruct.2018.10.058

Document Version
Peer reviewed version

Citation for published version (Harvard):
Janeliukstis, R, Clark, A, Papaelias, M & Kaewunruen, S 2019, 'Flexural cracking-induced acoustic emission peak frequency shift in railway prestressed concrete sleepers', *Engineering Structures*, vol. 178, pp. 493-505. https://doi.org/10.1016/j.engstruct.2018.10.058

Flexural cracking-induced acoustic emission peak frequency shift in railway prestressed concrete sleepers

Rims Janeliukstis[a*], Andrew Clark[b], Mayorkinos Papaelias[c], Sakdirat Kaewunruen[b,d]

[a] *Institute of Materials and Structures, Riga Technical University, Latvia, Riga, Ķīpsalas street 6*

[b] *Department of Civil Engineering, The University of Birmingham, United Kingdom, Birmingham, Pritchatts road*

[c] *School of Metallurgy and Materials, The University of Birmingham, United Kingdom, Birmingham, Elms road B15 2SE*

[d] *Birmingham Centre for Railway Research and Education, The University of Birmingham, United Kingdom, Birmingham, Pritchatts road 52*

* Corresponding author email: s.kaewunruen@bham.ac.uk

A novel technique for acoustic emission-based condition monitoring of railway prestressed concrete sleepers under flexural loading is established. The evolution of peak frequency of emissions under increasing loads is studied using data from four emission sensors. It is found that the bulk of emitted peak frequencies are clustered in three bands - [150-300] kHz, [300-460] kHz and [500-800] kHz in all cases of full-scale sleepers tested. Only slight variations of band ranges are observed. A correspondence of acoustic emission counts to a particular peak frequency is established. Not all emissions are damage-induced – most of them have relatively small number of counts, suggesting that those are due to random noise. Thus, it is proposed to filter out the non-significant peak frequencies with the least number of counts by applying a universal threshold rule. The largest proportion of emission counts corresponds to mid-span of the sleepers. It is shown that other acoustic emission sources exhibit a nearly linear shift in maximum values of peak frequency with increasing distance from this largest concentration of acoustic emission events. The novel insight into condition-based acoustic emissions is critical to develop a suitable and efficient technique for monitoring safety-critical railway sleepers and bearers located in a discreet and remote area. It will

truly enable predictive and condition-based track maintenance for railway industry, minimizing cost and environmental impacts.

Keywords: acoustic emission; concrete sleepers; counts; cracks; peak frequency; shift

Highlights

- Acoustic emissions are recorded from full-scale tests of prestressed concrete sleepers.
- Non-significant peak frequencies of emissions are filtered using a modified universal threshold.
- Maximum peak frequencies are assessed using emission counts and distribution centroid.
- Peak frequency shifts are nearly linear with distance from the main emission source.

1. Introduction

Railway sleepers are a safety-critical element of ballasted railway tracks. Among their many functions, the most important duty are to support and restrain the rails, to distribute loads from the rails to the underlying ballast, to maintain the rail gauge and shape, to withstand longitudinal, lateral and vertical movements of rails, to provide insulation between parallel rails, to resist wear, load and to endure extreme environmental conditions [1-6]. Timber was the first materials to be used in railway sleeper production due to relatively high availability, ease of installation and acceptable load bearing capacity. However, the most concern in the safe exploitation of timber sleepers lies in the fact that timber itself is susceptible to fungal decay and termite attacks. The common cause of timber sleeper failure is also end splitting [7]. Railway concrete sleepers were first introduced in railway infrastructure in 1950's. Nodaway's about 500 million railway sleepers are made of reinforced concrete [8-9]. Compared to their timber counterparts, concrete sleepers possess higher density and weight, thus providing more stability to railway tracks. Higher durability of the concrete also offers longer service life subject to static and dynamic loading [10].

During the services, concrete sleepers can develop different types of defects, resulting in structural failure [11]:

- bending cracks at the mid-span (center-bound failure) in transversal or diagonal direction due to shocks, improper infrastructure, drainage deficiency, poor track maintenance;
- breakage due to derailments or incorrect tamping (high intensity impact loading);
- cutting cracks at rail seat due to fatigue, reduced thickness of ballast, or improper infrastructure (low-cycle impact fatigue).

Ones of the most critical causes of concrete sleeper failure are the deterioration of concrete beneath the rail caused mostly by rail-seat abrasion and the installation or tamping damage [7-9]. Railway concrete sleepers also have to endure infrequent but high amplitude forces of short duration. Typically, loading due to wheel flats lasts 1 ms to 10 ms but the loading magnitude can reach as high as 600 kN per rail seat [12]. It is important to note that an individual failure of a sleeper will generally not cause disruption to rail operations but it will increase periodic track maintenance costs, increase costs and effort for safety-related track inspection and monitoring, and impair ride comfort of train passengers depending on the severity. Exceptionally, the failure of a sleeper will significantly increase the risk of rail breaks at welds, joints, rail surface defects, rail foot defects, turnouts (or called 'switches and crossings') [13], and will inevitably create asymmetrical load balancing and redistribution [14]. These exceptional risks can lead to detrimental train derailments causing not only financial penalties but also losses of lives [15].

Acoustic emission technique is now widely used for monitoring and damage detection in various engineering structures, such as concrete shear walls [16], concrete structures [17], railway sleepers [18], dams [19, 20], bridges [21-23], pavements [24, 25] and tunnels [26]. In principle, when a material is subjected to higher load, a burst of energy is released in the form of high-frequency elastic or shear waves from propagating cracks or from plastic deformation [16]. Acoustic emission sensors, mounted on the structure, record these waves upon their arrival from source and/or reflections. Various sources of acoustic emissions exist in concrete materials. The most prominent are cracking, friction due to aggregate interlock [27], de-bonding, etc. [27, 28]. In the cases of static or quasi-static loading, the two main failure

mechanisms in concrete are the tensile cracking and compressive crushing of the concrete [29]. In most cases, tensile failure mode takes place at smaller loads than shear failure [30]. The widely adopted method to improve the loading capacity, fracture characteristics and low tensile strength of the concrete [28, 29] is to incorporate prestressed tendons, which is particularly important for railway concrete sleepers.

Peak frequencies of emitted elastic and shear waves due to some damages such as corrosion or excessive loading are among the parameters that hold promise in damage detection and possible characterization. In [31], peak frequencies of acoustic emission in concrete mixtures with different water to cement ratio by mass were analyzed. It was found that three bands of frequencies can be discerned: [100-150] kHz, [150-200] kHz and [300-400] kHz. The researchers argued that the latter range is attributed to aggregate cracking. Feng and Yi [32] analyzed amplitude changes of emitted different frequency acoustic waves with the propagation distance from the source in reinforced concrete beam. They concluded that high frequency components attenuate rapidly and peak frequencies shift to lower values. They suggested that the frequency range of [200-250] kHz is more suitable for damage detection in reinforced concrete as emitted waves within this range do not decay as fast. Acoustic signals emitted from corrosion-induced damage in reinforced concrete beams were studied in [33]. The researchers suggested that peak frequencies of emitted waves are a good indicator of damage and observed three distinctive frequency parts: <50 kHz, ~110 kHz and >240 kHz. Studies in [34] suggest that the frequency range [180-350] kHz is attributed to formation of micro cracks and macro cracks with a short duration of emissions, while in [35] it is argued that peak frequencies in the range [275-350] kHz are a typical signature of concrete cracking. Peak frequency analysis was also conducted in [36] where concrete beams were loaded in tension and flexure and the peak frequency values of acoustic emission waved were weighted. Two clusters of weighted peak frequencies due to cracking were registered: [40-90] kHz and [120-200] kHz. In [30] acoustic emission signatures rising from defect formation in steel fibre reinforced concrete beams under bending were recorded. By the moment of maximum load, the majority of peak frequency values were in range [400-500] kHz, while after the load had dropped peak frequencies decreased to less than 400 kHz.

In this study, acoustic emission monitoring is employed for cracking characterization in railway prestressed concrete sleepers subjected to flexural loading. A set of full-scale concrete sleepers is loaded until failure, while the other set is used to identify cracking progression. This study proposes to filter non-significant peak frequencies of emissions due to noise by applying a modified universal threshold, a technique inspired by the research field of image analysis [37-39]. This novel procedure allows for compression of the acquired acoustic emission data considerably leaving only the signatures due to cracking and failure. Then, the relationship can be established between peak frequencies acquired from three emission sensors and the distance from these sensors to the main emission source at the mid-span of sleepers. Results suggest that this trend is nearly linear, although this fact cannot be clearly supported by linear regression due to large deviations in some cases.

The paper is organized as follows: Section 2 is devoted to the description of full-scale sleeper specimens, loading configurations and acoustic emission measurement details; Section 3 describes the peak frequency filtering process and two methods for extraction of peak frequencies to be later compared in terms of shifts with increasing distance from the main source of acoustic emission; Section 4 presents the results of sleeper loading in flexure and measured peak frequencies along with peak frequency filtering results for every acoustic emission channel (sensor) and the retained information after filtering; Section 5 deals with linear regression model applied to data of peak frequency vs distance from the main emission source; Section 6 is reserved for general conclusions of the scientific work.

2. Acoustic emission measurements

2.1 Sleeper setup for flexural loading

Four full-scale pre-stressed railway concrete sleepers kindly supplied by industry partner CEMEX are shown in Fig. 1(a). The characteristic length of sleepers is 2500 mm, depth at mid-span is 175 mm, depth at rail seat is 200 mm and width is 200 mm in accordance with CEMEX [40]. All supplied sleepers are manufactured from the same concrete mix and variability

of their mechanical properties does not exceed 3 %, thus minimizing the scatter in their performance on track. A single sleeper has a mass of 309 kg ± 3 kg for loose fastening components. A total of 6 pre-stressed reinforcing tendons are embedded within sleepers as shown in Fig. 1(b).

(a) (b)

Fig. 1. Pre-stressed railway concrete sleepers: (a) four sleepers. (b) cross-section showing 6 steel tendons.

European Standard BS EN 13230 [41] specifies the support conditions required for the three-point bending test (type testing), instructing point supports at the railheads for both positive and negative bending tests. The support must be 100 mm wide and made from steel with a hardness Brinell: HBW>240 as shown in Fig. 2.

Fig. 2. Railway concrete sleeper placed on steel supports for three-point bending procedure.

For this study, a static load is applied at the mid span of the sleepers for both positive and negative bending in accordance with BS EN 13230 [41]. Three-point bending generally assesses problems associated with centre bound failure of railway sleepers in the field. Fig. 3(a) and (b) illustrate the layout of the loading procedure for positive and negative bending moments respectively. Additionally, the figure illustrates the location of the various sensors. Inclinometer data has been analysed and published elsewhere and the data is not used in this study. A photograph showing locations of mounted **acoustic emission (**AE**)** sensors for positive bending configuration is shown in Fig. 3(c).

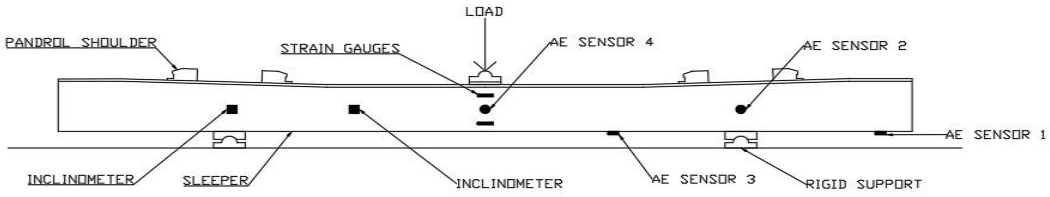

(a)

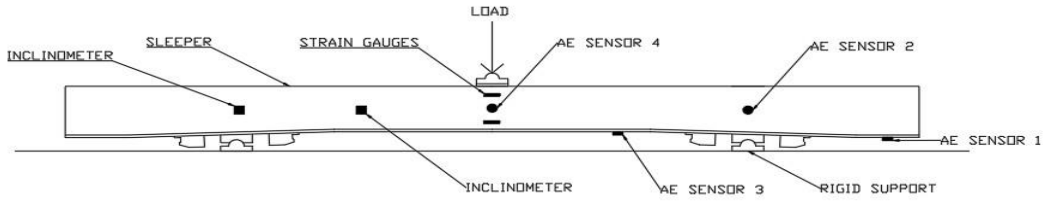

(b)

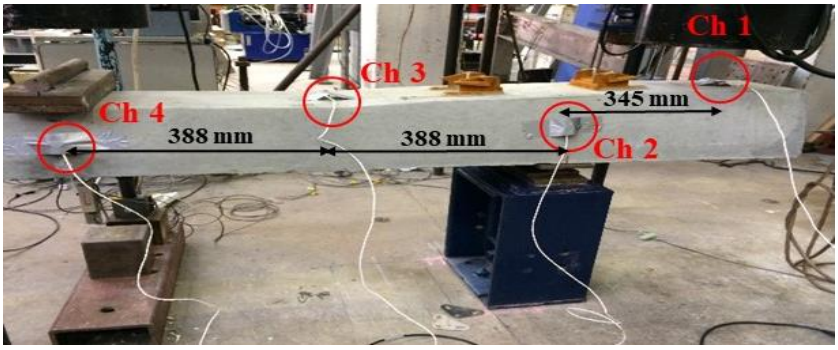

(c)

Fig. 3. Static loading layout for railway concrete sleepers in (a) negative and (b) positive bending configuration and location of AE sensors in (c).

2.2 Setup of acoustic emission system

AE measurements were carried out during the mechanical tests of all the specimen types to monitor and evaluate damage evolution during loading. The AE signals were detected and recorded using a 4-channel DAQ AE system procured from Physical Acoustics Corporation (PAC, now Mistras). The data acquisition was performed using "AE-Win" software. The AE signals were detected using wideband PAC-WD piezoelectric acoustic emission transducers operating at frequency range of 20-1000 kHz. The frequency response of these sensors allows the detection of AE signals over a wide frequency range. In this manner, the AE signal characteristics associated with the different failure modes can be assessed. In addition, each sensor is connected to PAC 2/4/6 preamplifier operating in the frequency bandwidth of 20-1200 kHz. The amplification level of the pre-amplifiers was set to 50 dB prior to testing. A higher amplification level would increase the noise content as well as the amplitude of the unwanted AE signals. In contrast, a lower amplification level would result in lower noise levels, but the damage related signals would not be sufficiently amplified. The AE sensors were coupled on the samples using Vaseline petroleum jelly and held in place with duct tape. The use of coupling agent removes the air between the sensor and the surface of the sample, ensuring effective transmission of the AE signals with limited signal loss. In contrast, poor coupling quality has an adverse effect on the transmission of the AE signals and leads to increased signal loss during the tests.

The data acquisition system used was a custom-built AE and vibration acquisition system capable of continuously recording the complete waveform for periods of few seconds. The custom-built acquisition system consisted of the following components:

- A computer with a customised data logging software;
- An Agilent U2531A 4 channel data acquisition card;
- A 4 channel decoupling hub;

- A MISTRAS Wide bandwidth AE amplifier provided by PAC;
- A PAC model 2/4/6 preamplifier operating in the frequency range of 20-1200 kHz;
- Wideband PAC-WD piezoelectric AE sensors operating in the frequency range of 20-1000 kHz.

3. Peak frequency filtering and shift assessment

The generation of acoustic emission events due to breakage of bonds between particles of material occurs at specific frequency regions or bands. At increased loading, defects (cracks in concrete) propagate, increasing the range of emitted frequencies (frequency shifting). This ideology of characteristic frequencies of defect formation in the structure can be compared to inherent resonant frequencies of the structure in terms of resonant frequency changes due to damage. For example, by conducting modal analysis for some structure, resonant frequencies are obtained. These frequencies shift if some sort of damage is present and the magnitude of shift is dependent on damage severity and size.

Acoustic emissions with a wide array of different peak frequency values are recorded during the loading process. Some of these frequencies are characteristic of noise. However, the events of formation of damage usually emit waves characterized with a relatively massive amount of emission counts. As the number of broken atomic bonds increases, the number of hits and counts that represent the emitted elastic waves also increases. Peak frequency of an acoustic emission waveform is chosen as a damage-sensitive parameter. Peak frequency is a frequency that corresponds to a maximum amplitude of Fourier Transform of acoustic emission waveform. Peak frequency is a reliable indicator of different acoustic emission sources [34], including corrosion of concrete reinforcement and load-induced cracking.

The purpose of this study is to filter out insignificant peak frequencies of acoustic emissions – the ones that are, most likely, not associated with the events of cracking in prestressed railway concrete sleepers. As a tool for such a filtering, the universal threshold T, introduced by Donoho is adopted for modification. Originally, this threshold was adapted in image noise reduction routine by using wavelets [37-39].

$$T = \sigma\sqrt{2\ln(N)} = \frac{MAD}{0.6745}\sqrt{2\ln(N)} = \frac{Median|x_i - Median(x_i)|}{0.6745}\sqrt{2\ln(N)} \quad (1)$$

where σ denotes the standart deviation of noise and N is the number of samples in the signal. The term σ is calculated through MAD – Median Absolute Deviation term that, in turn, is the median value of the absolute differnece between every sample of the signal and it`s median. The value of 0.6745 in the denominator makes the estimate unbiased for the normal distribution [30]. The modification procedure is as follows:

1. A total number of counts is summed for every value of peak frequency recorded throughout the whole acoustic emission interrogation process for every channel of every sleeper.
2. The universal threshold from Eq. (1) is applied to all count values and only the ones that exceeed the threshold are retained. Others are discarded.
3. A new set of peak frequency and corresponding count pairs is formed based on the filtering in the previous step (see Fig. 6, 10, 13, 16). From this set, the peak frequency corresponding to maximum number of counts is registered.
4. Using the filtered peak frequency-counts sets, the centroid value of peak frequency PFC is computed using the formula in analogy to center of mass for a body

$$PFC = \frac{\sum_i^N C_i \times PF_i}{\sum_i^N C_i} \quad (2)$$

where C– counts and PF– peak frequency. For every sample i the number of counts is multiplied by the corresponding peak frequency and all such multiplications are summed up for all samples N. This summation is then divided by the sum of all counts. The calculation is done in order to evaluate the location of largest proportion of counts in terms of peak frequency and compare this to the one corresponding to maximum counts.

5. A linear regression model of peak frequency shifts with distance from the main acoustic emission source at the mid-span of the sleepers is made for both approaches – peak frequencies corresponding to maximum number of counts (step 3) and centroid values of peak frequencies obtained from step 4.

4. Peak frequency analysis

4.1 Negative bending to failure

The first crack of the sleeper is marked at 70 kN load. The marking of crack progression (shown in Fig. 4) was ceased above the load of 98 kN (when concrete crushing starts) for the safety of testing personnel since severe cracking and possible failure was imminent at any moment. The failure load is registered at 102 kN. At the moment of failure, a deflection of 17 mm is registered at the mid-span. The failure mode is mixed (flexural + shear), which confirms the results of previous studies [42].

Fig. 4. Failure pattern of sleeper 1.

The evolution of peak frequencies corresponding with loading, along with load-deflection curves, is shown in Fig. 5. No distinct emission burst is observed at the event of the first crack. However, the most intense emissions correspond to the event of failure and even after that. According to [31], a somewhat similar phenomenon was observed – the amount of acoustic emission energy released before peak load

was less than 10 % of the total emitted energy. Farnam et al. [31] explained that the reason of small fraction of acoustic emissions at the initial cracking may be due to the formation of small micro cracks with relatively small surface areas. In this study, emission events are clearly dominated by the ones coming from mid-span (channel no. 4) with a range of peak frequencies from 150 kHz to about 600 kHz. Three distinctive bands of peak frequencies are registered – [150-300] kHz, [385-460] kHz and [498-496] kHz as indicated from Fig. 5. Emissions from channels no. 1 and 2 occur at the lowest frequency band [150-300] kHz.

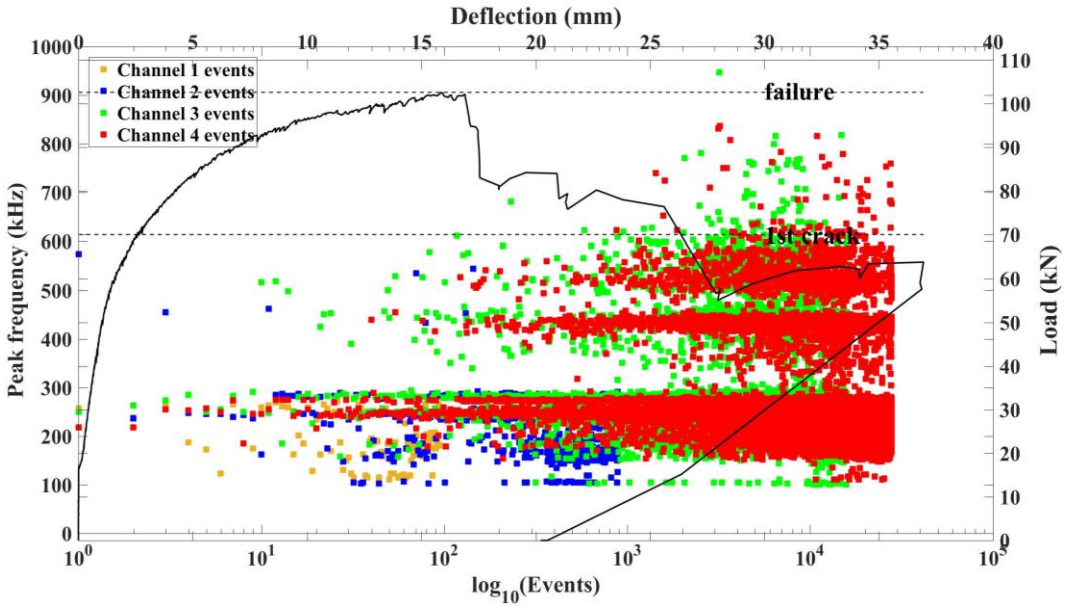

Fig. 5. Peak frequency evolution for sleeper 1.

The results of peak frequency filtering are shown in Fig. 6. Apparently, the maximum number of counts greatly exceeds the threshod value. For channel no. 1, this difference is 19 times. The differences of 20 times, 48 times and 266 times for channels no. 2, 3 an 4, respectively, are registered. The peak frequency filtering technique allows to significantly reduce the number of peak frequencies for further analysis. In the case of sleeper 1, only 20 %, 18 %, 22 % and 28 % of peak frequency values are retained for channels no. 1, 2, 3 and 4, respectively. Bar plots of retained peak frequency-count pairs are shown as

inlet plots in Fig. 6, 10, 13, 16. After the filtering, the effective peak frequency range is decreased and this effect is more pronounced for channel no. 4 with the largest proportion of emissions. For channel no. 1 the peak frequency range [111-271] kHz is filtered to [119-265] kHz, whereas for channel no. 4 – from [111-837] kHz to [160-529] kHz.

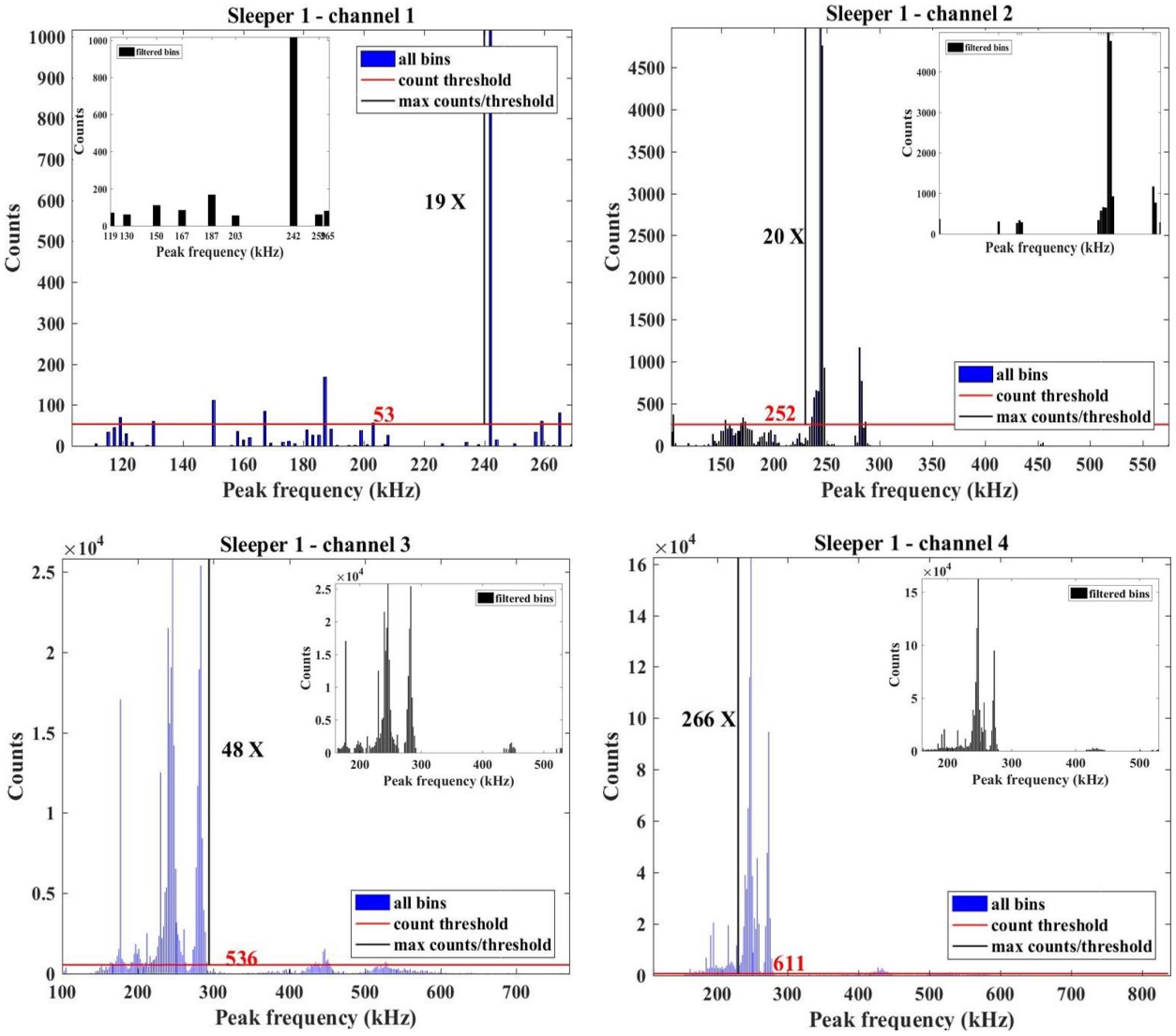

Fig. 6. Peak frequency filtering for sleeper 1.

4.2 Negative bending crack progression

The sleeper no. 2 and similarly sleeper no. 4 are loaded until the first crack and unloaded. Then, the applied load is again increased from 0 kN to a load roughly corresponding to 1.5 times the load of the first crack. During both loading phases, acoustic emissions are recorded. The first crack for sleeper no. 2 occurs at load of 53 kN as shown in Fig. 7. The cracking progression is shown in Fig. 8.

Fig. 7. The first crack of sleeper 2.

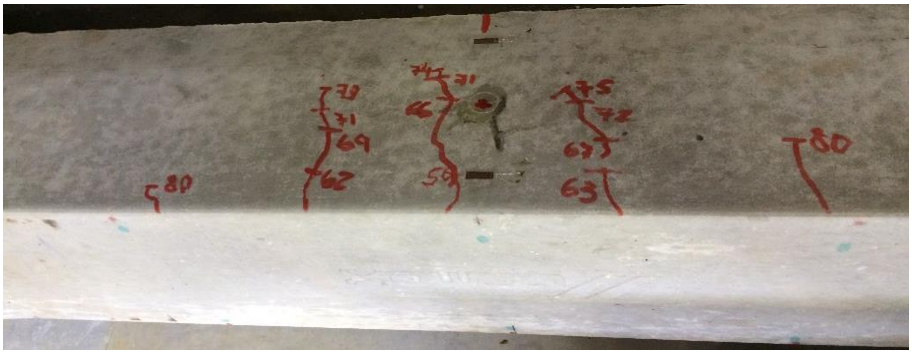

Fig. 8. Crack progression of sleeper 2.

The load-deflection curves overlayed with peak frequency evolution with loading are depicted in Fig. 9. The total deflection at the highest load is about 3.5 mm. Again, three distinct peak frequency bands are present with the most contribution from channel no. 4. The bands are [140-290] kHz, [360-440] kHz and [500-600] kHz. The emissions from other channels are barely visible with an exception of channel no. 3. ~~Although the emissions from this channel last throughout the whole test, these emisisons are scattered in~~

~~time – relatively low number of events are present in the range [120-610] kHz.~~ Emissions from channels no. 1 and 2 are mostly associated with lower frequency band of [140-290] kHz.

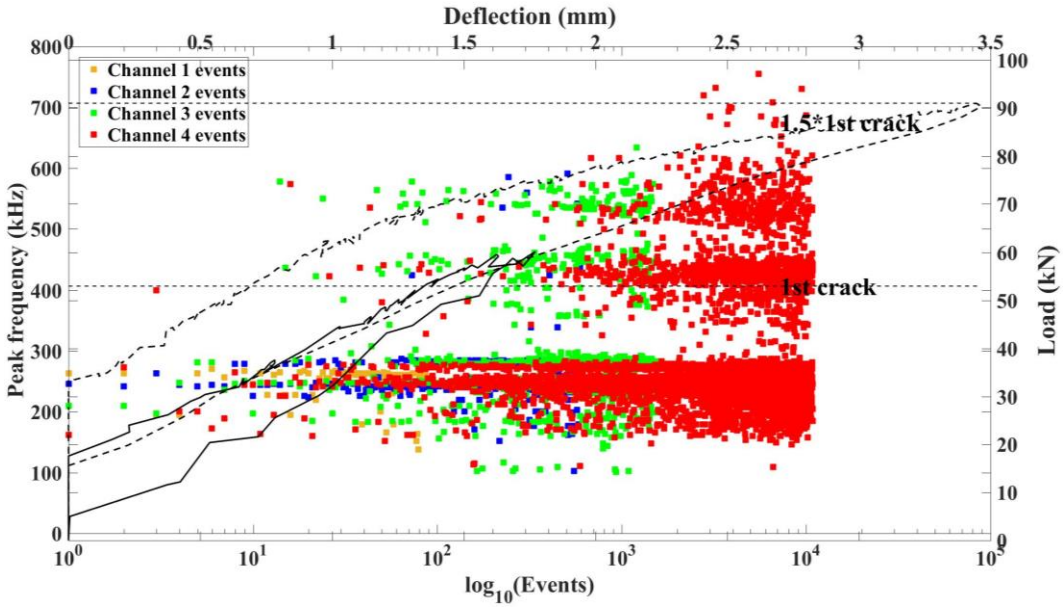

Fig. 9. Peak frequency evolution for sleeper 2.

Peak frequency filtering results are shown in Fig. 10. Only 4 out of 23 peak frequencies are significant for channel no. 1, while 65 out of 256 for channel no. 4. The count information retained is 67 % and 91 %, respectively. This result indicates the possibility of significant data compression for analysis of acoustic emission phenomena. As with the cases for other sleepers, large difference between threshold value and maximum number of counts can be observed – ranging from 5 times for channel no. 1 to 57 times for channel no. 4.

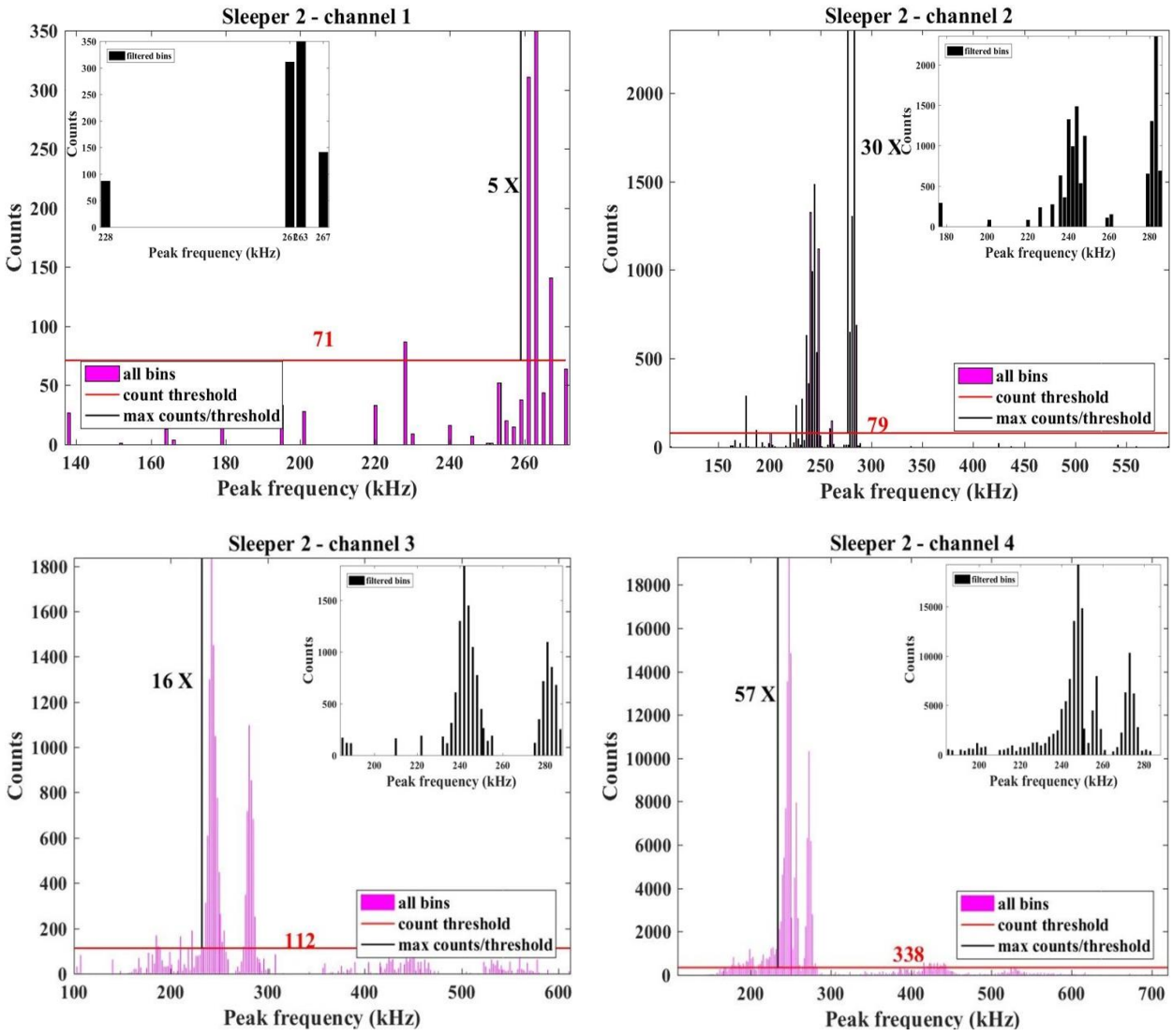

Fig. 10. Peak frequency filtering for sleeper 2.

4.3 Positive bending to failure

Subject to the positive bending moment, the first flexural crack occures at load of 53 kN, while the failure of the sleeper is registered at load of 113 kN. The failure mode is in pure shear. The failure is characterized with substantial loss of concrete mass as can be seen in Fig. 11. The total deflection of sleeper at mid-span at the moment of failure is about 7.7 mm.

Fig. 11. Failure pattern of sleeper 3.

Three bands of peak frequency values are clearly seen in Fig. 12. The widest band is [150-300] kHz, the second band is [350-450] kHz and the third band is [500-600] kHz. Acoustic emission events are clearly dominated by channel no. 4 characterized by highest density of cracks. As with sleepers no. 1 and 2, acoustic emissions from channels no. 1 and 2 mostly occur at the lowest frequency band of [150-300] kHz. Significant emission bursts correspond to the stage of failure. Emissions from other channels are much less pronounced. Different emisison frequencies correspond to different failure mechanisms – at the loading stage near failure the acoustic emisison events are due to tensile matrix micro-cracking, while fiber pull-out takes place after the formation of main cracks, in accordance with [33].

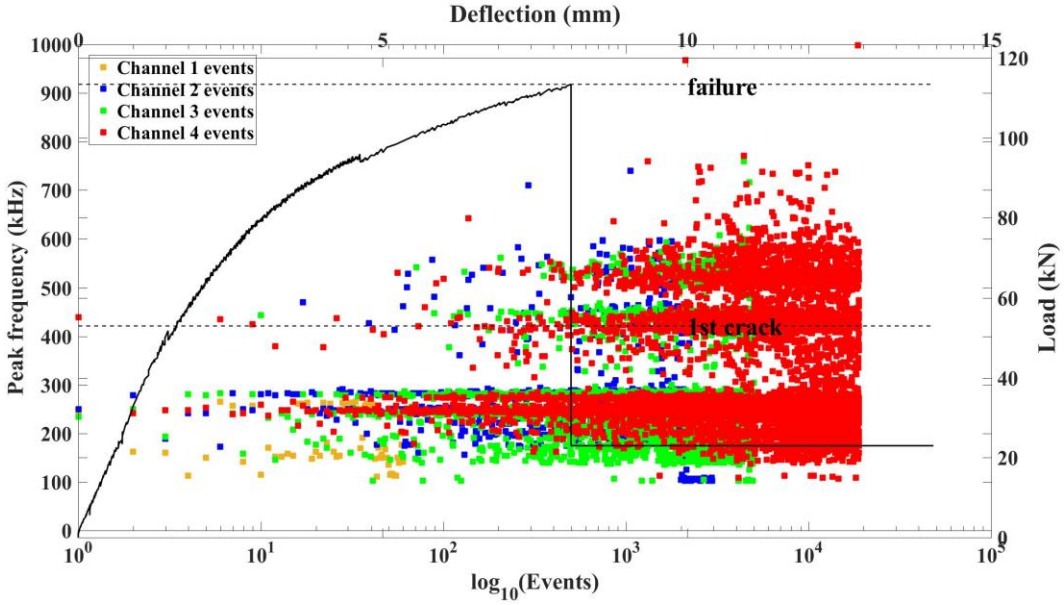

Fig. 12. Peak frequency evolution for Sleeper 3.

Peak frequency distributions and filtering results for sleeper no. 3 are shown in Fig. 13. Atypical data compared to other channels and channels of other sleepers is the result for channel no. 1. It shows that maximum number of counts corresponds to peak frequency of 140 kHz, while in all ather cases this value is about $(250 \pm 10)\ kHz$. Large differences between established threshold values and maximum bumber of counts can be observed for this sleeper. Also, there is a trend for increasing threshold with decreasing distance to mid-span (from channel no. 1 to channel no. 4). The most prominent reduction in peak frequency range after filtering is observed for channel no. 3 and 4 – from [103-759] kHz to [142-447] kHz for channel no. 3 and from [107-998] kHz to [169-527] kHz for channel no. 4.

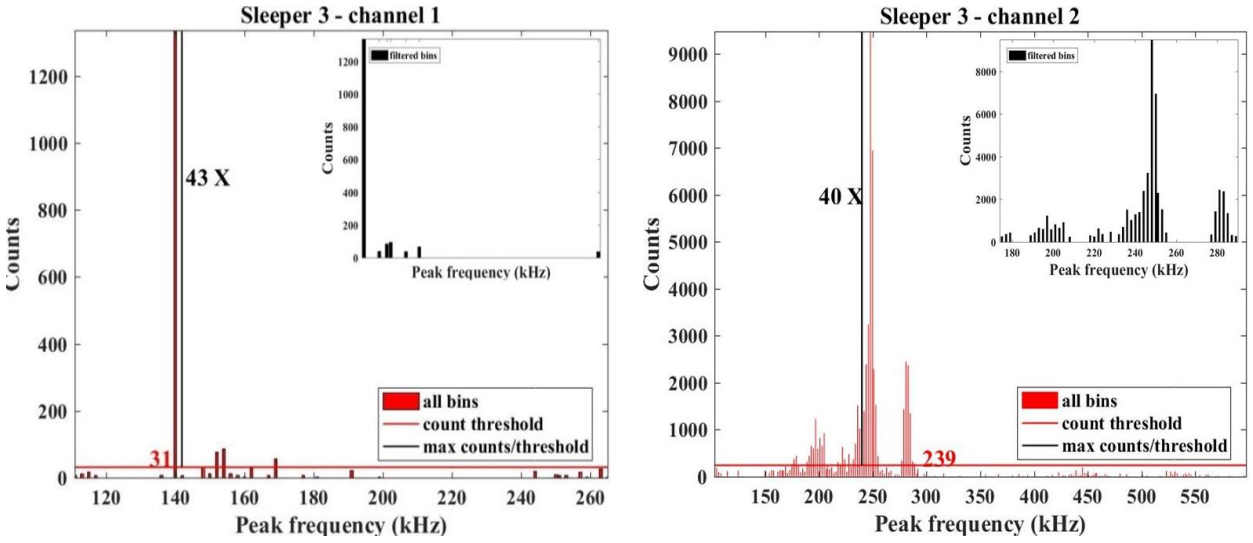

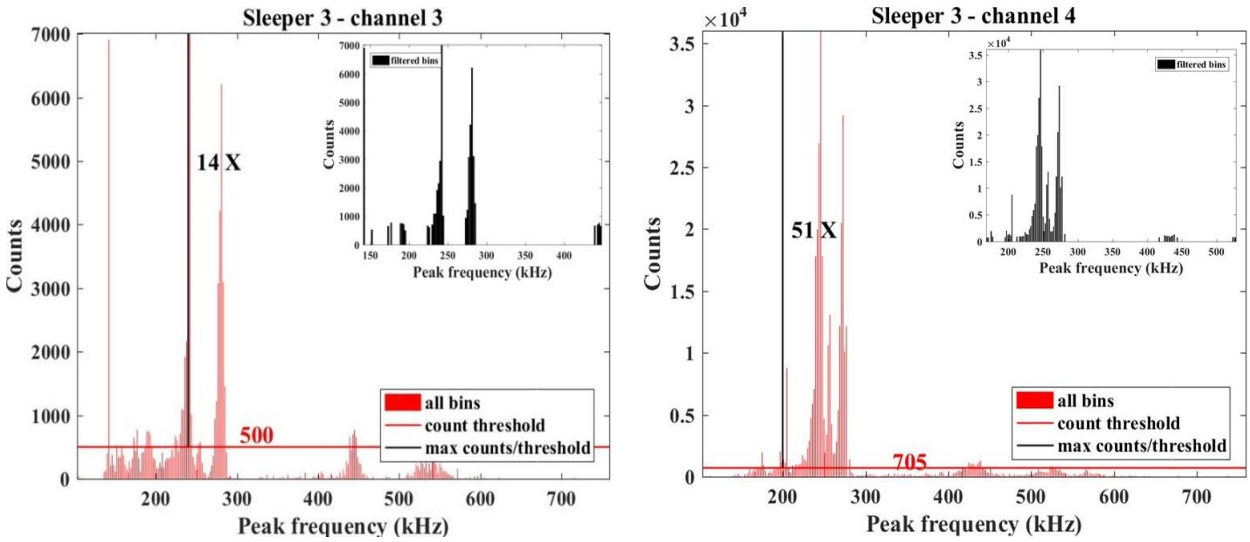

Fig. 13. Peak frequency filtering for sleeper 3.

4.4 Positive bending crack progression

The first crack under the positive bending moment is registered at load of 53 kN. The loading is proceeded until the load of approximately 83 kN as shown in Fig. 14. During the initial loading phase the deflection of the sleeper is only 1 mm, while the total deflection is about 4 mm as recorded by LVDT. The load-deflection curves along with peak frequency evolution during loading are shown in Fig. 15.

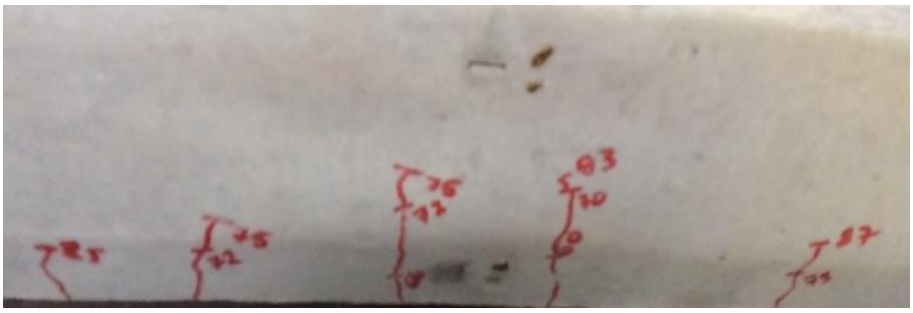

Fig. 14. Cracking pattern of sleeper 4.

Surprisingly, the increase of peak frequency values of channel no. 2 is the most pronounced with increasing load with the ladder-like signature ~~in time domain~~ and comparatively few ~~number of~~ emission

events. Relatively lower peak frequencies are emitted in the vicinity of channel no. 4 – the band is [100-300] kHz and there are relatively few events in this channel, although the emissions have lasted through out the whole test. The dominating proportion of events are emitted near channel no. 3 where a range of frequencies is wide with 3 distinct bands [150-300] kHz, [300-460] kHz and [500-700+] kHz. Very few emisisons from channel no. 1 are registered and mostly attributed to the lowest frequency band [150-300] kHz.

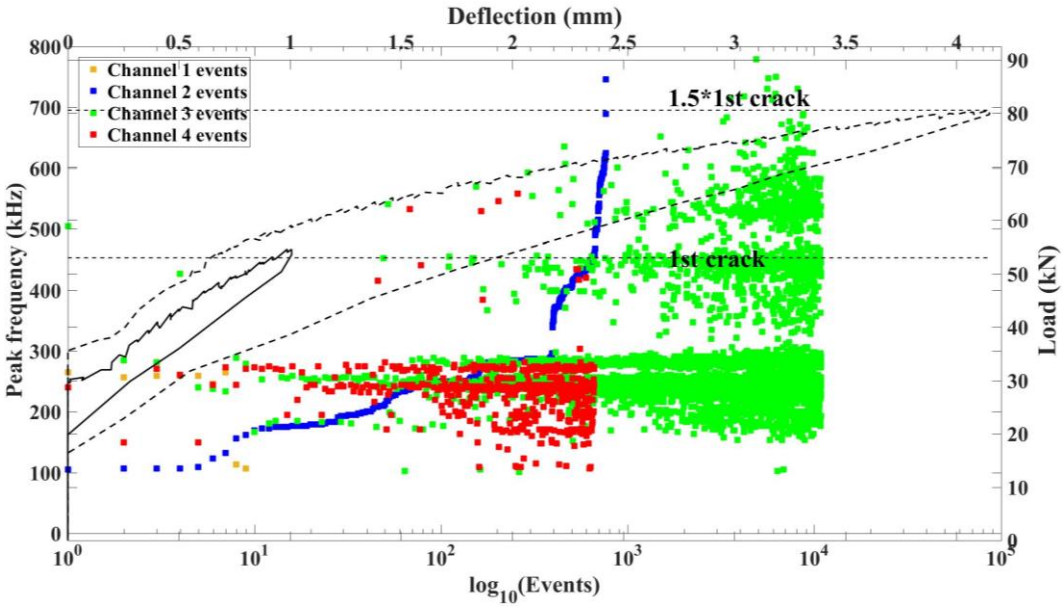

Fig. 15. Peak frequency evolution for Sleeper 4.

The results of peak frequency filtering for all 4 channels are shown in Fig. 16. Only 6 peak frequency values are detected in channel no. 1. The largest number of counts is 2 times larger than threshold value of 79, thus only 1 significant value of 259 kHz peak frequency is retained. For channel no. 2, only 14 % of all values remain after filtering with largest number of counts at 287 kHz peak frequency. The largest difference of 36 times between threshold value and the largest count peak is for channel no. 3. Peak frquency corresponding to the most counts is at 248 kHz and only 18 % of all peak frequency values are

significant in this case. Acoustic emisisons with a peak frequency of 240 kHz have generated the most counts at the mid-span. Only 14 out of 87 different peak frequency values are significant.

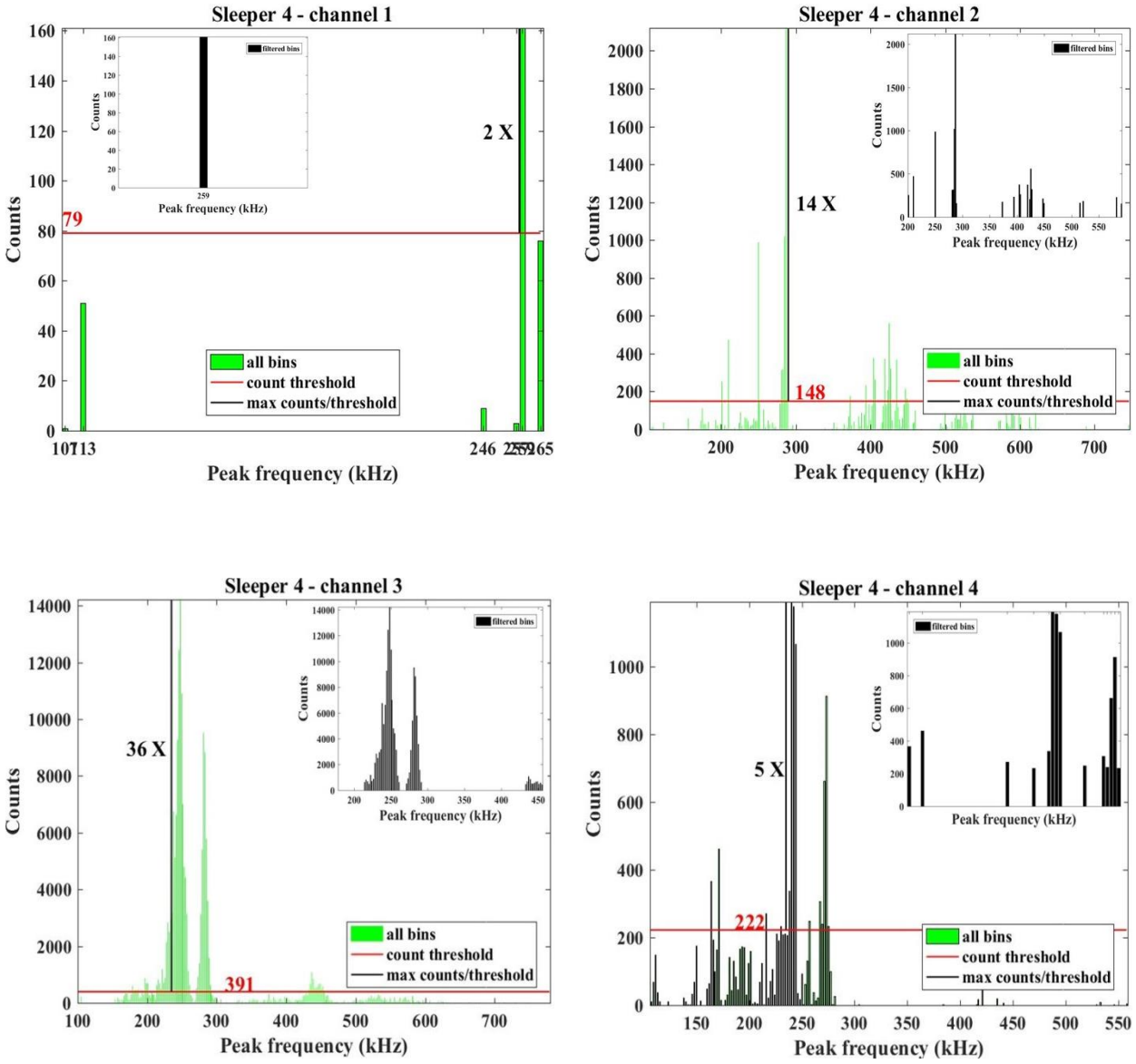

Fig. 16. Peak frequency filtering for sleeper 4.

The results summarizing the raw peak frequency/counts data and the information retained after the filtering are shown in Table 1. It is clear that the universal threshold value increases by decreasing the distance from channel no. 1 to channel no. 4. In short, the intensity of acoustic emissions had increased in

the direction towards the mid-span of the sleepers. The only exception is sleeper no. 4. For all of the channels, the proportion of significant peak frequencies constitute only 14 % to 34 % of the initial data with 53 % to 98 % count information retained. This insight is critical for modified universal thresholds that are suitable for local placement of sensors. Overall, the total range of peak frequencies recorded in the events of acoustic emissions is from 101 kHz to 998 kHz. This is an ultrasound range. The largest variety of different peak frequencies is emitted mostly at mid-span. After the application of modified threshold, the peak frequency range, so-called ‘effective peak frequency’, has decreased – 105 kHz to 591 kHz. In addition, the farthest end of recorded peak frequency spectrum has insignificant number of counts and thus 592 kHz to 998 kHz values are discarded.

Table 1

Results of remaining information after counts filtering using universal threshold.

Channel no.	Full			Filtered			Remaining (%)			Threshold
	Bins	Counts	Range (Hz)	Bins	Counts	Range (Hz)	Bins	Counts	Range	
Sleeper 1										
1	44	2228	111-271	9	1709	119-265	20	77		53
2	85	21767	103-574	15	16667	105-287	18	77		252
3	302	307246	101-947	67	280512	164-529	22	91		536
4	289	1012949	111-837	82	988526	160-529	28	98		611
Sleeper 2										
1	23	1328	138-271	4	889	228-267	17	67		71
2	53	13257	103-591	18	12674	177-285	34	96		79
3	170	17918	101-634	25	13499	185-287	15	75		112
4	256	160494	109-755	65	146324	169-529	25	91		338
Sleeper 3										
1	31	1965	111-265	7	1706	140-263	23	87		31
2	178	58226	103-740	38	50736	175-289	21	87		239
3	204	77305	103-759	29	53777	142-447	14	70		500
4	293	358301	107-998	57	318029	169-527	19	89		705
Sleeper 4										

Channel no.	Full			Filtered			Remaining (%)			Threshold
	Bins	Counts	Range (Hz)	Bins	Counts	Range (Hz)	Bins	Counts	Range	
1	6	301	107-265	1	161	259	17	53		79
2	156	14614	105-746	22	9261	201-591	14	63		148
3	263	177646	101-779	48	154327	214-455	18	87		391
4	87	12370	107-558	14	7714	164-275	16	62		222

5. Linear modeling of peak frequency shifts

The results of linear fitting of peak frequency values vs distance from the main source of acoustic emissions are presented in Fig. 17. A common least-squares fitting procedure is adopted [43]. As one can see, the relationship is nearly linear. MAD value from Eq. (1) is shown (depicted by s), representing deviations from median value. Large deviations are present, in particular, for sleeper no. 4. This is due to the fact that, surprisingly, the highest density of acoustic emissions is registered not at mid-span but at channel no. 3 instead (see Table 1). As for sleeper no. 3, one outlier point is detected – for channel no. 1 (Fig. 17(a)) and channel no. 4 (Fig. 17(b)). One also sees that both methods display somehow contradictory results in terms of increasing or decreasing shift with increasing distance. On Fig. 17(a) the trend is increasing for sleepers no. 2 and 4, while it is decreasing for sleepers no. 1 and 3. On Fig. 17(b) the results are opposite. This insight informs that predicted modes of failure should be consistent to the placement of sensors. It is clear that the results conform exceptionally well for the sleepers failing in bending and mixed bending shear modes. In contrast, the acoustic emission intensity will be directed to the nearest sensors as clearly evident in the cases of sleepers failing in brittle or pure shear modes.

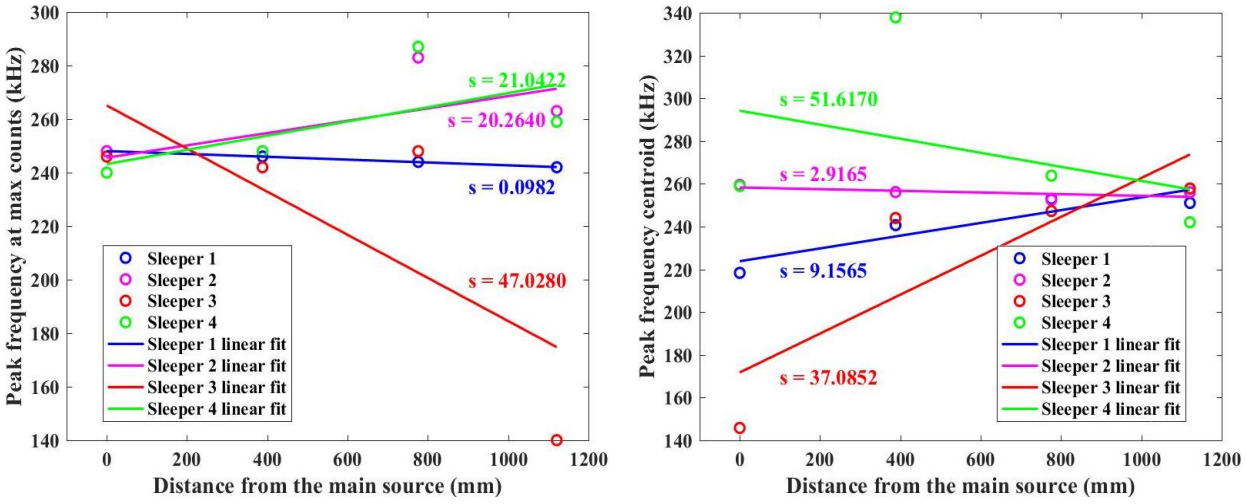

(a) (b)

Fig. 17. Linear fits of relationship between peak frequency and distance from the main source of emissions at mid-span: (a) peak frequency corresponding to maximum counts; (b) centroid value of peak frequency.

The intercept and slope terms of a linear model fit from Fig. 17 are shown in Table 2. The sign of slopes is opposite using both methods. The intercept values do not differ significantly, except for sleepers no. 3 and 4. In general, it can be estimated that the trends are linear; however, relatively large outliers are present in most cases. Also, there is no consistency between both shift assessment methods in terms of increasing or decreasing relationship between peak frequencies and distance from the main emission source. The most reliable fit is obtained for sleeper no. 1 by considering peak frequencies at maximum number of counts. The trend is for peak frequencies to decrease slightly with increasing distance from the largest emission bursts.

One of the most important factors influencing the proposed methodology monitoring the crack propagation in railway sleepers is boundary conditions. The experiments were conducted in simply supported conditions adjusted for three-point bending tests. Of course, in a real railway track sleepers are embedded in a ballast bed which is free support condition. In this case, the distribution of mechanical stresses is also different influencing the formation of defects (cracks). However, most cracking in railway concrete sleepers occur at mid-span [11] anyway which is in accordance with our experimental results.

Another factor influencing the results is maintenance of a railway track. If the AE system is to be set in a real railway track, AE sensors will record the AE signal coming from sleepers subjected to dynamic loading of the passing trains. A practical solution for real in situ applications is to employ wireless sensors which are already commercially available [44]. In this case, the complicated wiring issue and parasitic inductance stemming from the excessive wiring is avoided. Thus, monitoring of the crack propagation using the proposed method can be achieved. Nevertheless, if the railway track is not maintained properly, degradation of sleepers can occur due to environmental conditions (temperature changes, moisture, etc.) and make an undesirable impact on the monitoring results.

Table 2

Coefficients of linear fitting model.

Shift assessment method	**Sleeper 1**		**Sleeper 2**		**Sleeper 3**		**Sleeper 4**	
	Slope	Intercept	Slope	Intercept	Slope	Intercept	Slope	Intercept
max counts	-0.0053	248	0.023	246	-0.081	265	0.024	243
centroid	0.030	224	-0.0039	258	0.091	172	-0.033	294

6. Conclusions

The changes of peak frequency of acoustic emission events in railway prestressed concrete sleepers subjected to static flexural loads are evaluated and analyzed. A total of four full-scale sleepers each equipped with four acoustic emission sensors are tested. Two sleepers are loaded till failure and the other two examined in terms of cracking progression. A wide variety of peak frequency values is registered with over 5 million data points. The range is consistently within [101-998] kHz. In the cases for all four concrete sleepers, the recorded evolution of peak frequencies with increased loading suggests that most of

the peak frequency values cluster around three bands with the following average values over all sleepers: [150-300] kHz, [300-460] kHz and [500-800] kHz.

However, not all af these peak frequencies are due to formation of cracks, crack propagation and failure – a fair proportion is due to noise. In this study, it is proposed to apply a modified filtering to filter out insignificant peak frequencies – those having low number of emission counts. A modified universal threshold technigue is established for filtering. All peak frequencies with corresponding counts lower than the threshold are rejected. The filtering results suggest that it is possible to retain 14 % to 34 % of initially recorded peak frequencies, while retaining count information to the extent of 53 % to 98 % of the initial number of counts. Hence, most data can be rejected and the most important information pertinent to structural health of railway concrete sleepers still maintained. The new findings show that the modified universal treshold is suitable for monitoring structural integrity of railway sleepers. This is because general track inspections cannot precisely identify modes of failure and the use of modified threshold can be more adaptive to the actual modes of failure of the sleepers in the field.

The second part of this study attempts to establish a linear relationship between maximum value of retained peak frequencies and distance from the main source of acoustic emissions, which happens to be at or adjacent to mid-span for almost all sleeper cases. Centroid of retained peak frequency ditributions (earlier shown in Fig. 6, 10, 13 and 16) is calculated to evaluate the location of largest proportion of counts in terms of peak frequency. This value is calculated for all four acoustic emission channels for every sleepr. A linear regression model is built where maximum values of retained peak frequencies and peak frequency centroids versus distance from mid-span are fitted to linear function. The results reasonably suggest that the relationship is fairly linear, however, strong outliers are present in some cases contributing to significant deviations from linearity. Perhaps, this scatter could be decreased by considering more sleeper specimens. Even though the variability of material properties of the sleepers does not exceed 3 %, the statistical confidence would benefit from increased sample size. This was, however, not done due to the nature of of specimens themselves (mass and size), as well as imposed limitations on sleeper shipment. Fitted linear models using both methods (maximum of retained peak

frequency and peak frequency centroid) do not match in terms of slopes – one method displays increasing trend, while the other shows decreasing relationship. This implies that the mode of failure in each case is different. Then, the best fit in terms of the smallest deviation from linearity can be achieved using maximum of retained peak frequency towards the nearest sensor. This insight will significantly help the development of an acoustic emisison sensor system that can accurately inform mode of failure and fragility tensors. It will revolutionise the structural health monitoring system of railway networks, particularly at discreet and remote locations such as swithes and crossings.

Acknowledgements

The research leading to these results was partially supported by the Latvia State Research Programme under grant agreement "Innovative Materials and Smart Technologies for Environmental Safety, IMATEH". The last author wishes to gratefully acknowledge the Japan Society for Promotion of Science (JSPS) for his JSPS Invitation Research Fellowship (Long-term), Grant No L15701, at Track Dynamics Laboratory, Railway Technical Research Institute and at Concrete Laboratory, the University of Tokyo, Tokyo, Japan. The JSPS financially supports this work as part of the research project, entitled “Smart and reliable railway infrastructure”. The authors are very grateful to European Commission for H2020-MSCA-RISE Project No. 691135 “RISEN: Rail Infrastructure Systems Engineering Network” (www.risen2rail.eu). Gratitude is due to Chayut Ngamkhanong for his help and contributed knowledge to the experiment. In addition, the sponsorships and assistance from CEMEX, Network Rail, and RSSB (Rail Safety and Standard Board, UK) are highly appreciated.

References

[1] C. Esveld, *Modern Railway Track*, The Netherlands MRT Press. (2001).

[2] B. Indraratna, C. Rujikiatkamjorn, and W. Salim, Advanced Rail Geotechnology – Ballasted Track, CRC Press, London, UK (2011).

[3] A.M. Remennikov, S. Kaewunruen, Experimental Investigation on Dynamic Railway Sleeper/Ballast Interaction, *Exp. Mech.* **46** (2006) 57–66, doi: 10.1007/s11340-006-5868-z.

[4] A.M. Remennikov, S. Kaewunruen, "Determination of prestressing force in railway concrete sleepers using dynamic relaxation technique," ASCE Journal of Performance of Constructed Facilities, 29(5), 04014134:1-7 (2015). doi: 10.1061/(ASCE)CF.1943-5509.0000634

[5] R. Gustavson, Structural behaviour of concrete railway sleepers. PhD Thesis, Department of Structural Engineering, Chalmers University of Technology, Sweden (2002).

[6] A.M. Remennikov, S. Kaewunruen, Experimental load rating of aged railway concrete sleepers, Engineering Structures, 76: 147-162 (2014). doi: 10.1016/j.engstruct.2014.06.032

[7] W. Ferdous, A. Manalo, Failures of mainline railway sleepers and suggested remedies – Review of current practice, *Eng. Fail. Anal.* **44** (2014) 17-35, doi: 10.1016/j.engfailanal.2014.04.020.

[8] R. You, D. Li, C. Ngamkhanong, R. Janeliukstis and S. Kaewunruen, Fatigue life assessment method for prestressed concrete sleepers. Front. Built Environ. 3:68. (2017) doi: 10.3389/fbuil.2017.00068

[9] É.A. Silva, D. Pokropski, R. You, S. Kaewunruen, Comparison of structural design methods for railway composites and plastic sleepers and bearers, Australian Journal of Structural Engineering, 18(3): 160-177 (2017). doi: 10.1080/13287982.2017.1382045

[10] N.O. Bezgin, High performance concrete requirements for prefabricated high speed railway sleepers, *Constr. Build. Mater.* 138(1) (2017) 340-351, doi: 10.1016/j.conbuildmat.2017.02.020.

[11] J.A. Zakeri, F.H. Rezvani, Failures of Railway Concrete Sleepers During Service Life, *Int. J. Constr. Eng. Manag.* **1**(1) (2012) 1-5, doi: 10.5923/j.ijcem.20120101.01.

[12] S. Kaewunruen, A.M. Remennikov, Experiments into impact behavior of railway prestressed concrete sleepers, *Eng. Fail. Anal.* **18** (2011) 2305-2315, doi: 10.1016/j.engfailanal.2011.08.007.

[13] S. Kaewunruen, Monitoring in-service performance of fibre-reinforced foamed urethane sleepers/bearers in railway urban turnout systems, Structural Monitoring and Maintenance, 1(1): 131-157 (2014), doi: 10.12989/smm.2014.1.1.131

[14] S. Kaewunruen, A.M. Remennikov, Effect of a large asymmetrical wheel burden on flexural response and failure of railway concrete sleepers in track systems, Engineering Failure Analysis, 15(8): 1065-1075, doi: 10.1016/j.engfailanal.2007.11.013

[15] S. Dindar, S. Kaewunruen, M. An, J.M. Sussman, Bayesian Network-based probability analysis of train derailments caused by various extreme weather patterns on railway turnouts, Safety Science, (2017) in press, doi: 10.1016/j.ssci.2017.12.028

[16] A. Farhidzadeh, S. Salamone, B. Luna, A. Whittaker, Acoustic emission monitoring of a reinforced concrete shear wall by b-value–based outlier analysis, *Struct. Health. Monit.* **12**(1) (2012) 3-13, doi: 10.1177/1475921712461162.

[17] B. Omondi, D.G. Aggelis, H. Sol, C. Sitters, Improved crack monitoring in structural concrete by combined acoustic emission and digital image correlation techniques, *Struct. Health. Monit.* **15**(3) (2016) 359-378, doi: 10.1177/1475921716636806.

[18] A. Clark, S. Kaewunruen, R. Janeliukstis, M. Papaelias, Damage detection in railway prestressed concrete sleepers using acoustic emission, IOP Conference Series: Materials Science and Engineering 251 (1), 012068, doi: 10.1088/1757-899X/251/1/012068

[19] C. Houqun, W. Shengxin, D. Faning, Experimental study of dynamic and static damage failure of concrete dam based on acoustic emission technology, Seismic Safety of High Arch Dams, Chapter 13, Academic Press (2016) 321-394.

[20] O. Minemura, N. Sakata, S. Yuyama, T. Okamoto, K. Maruyama, Acoustic emission evaluation of an arch dam during construction cooling and grouting, *Constr. Build. Mater.* 12(6-7) (1998) 385-392, doi: 10.1016/S0950-0618(97)00082-2

[21] A. Nair, C.S. Cai, Acostic emission monitoring of bridges: Review and case studies, *Eng. Struct*. **32**(6) (2010) 1704-1714, doi: 10.1016/j.engstruct.2010.02.020.

[22] B. Goszczyńska, G. Świt, W. Trampczyński, Application of the IADP acoustic emission method to automatic control of traffic on reinforced concrete bridges to ensure their safe operation, *Arch. Civ. Mech. Eng.* **16**(4) (2016) 867-875, doi: 10.1016/j.acme.2016.06.003.

[23] J.E. Parks, T. Papulak, C.P. Pantelides, Acoustic emission monitoring of grouted splice sleeve connectors and reinforced precast concrete bridge assemblies, *Constr. Build. Mater.* **122**(30) (2016) 537-547, doi: 10.1016/j.conbuildmat.2016.06.076.

[24] Z. Sun, B. Behnia, W.G. Buttlar, H. Reis, Assessment of low-temperature cracking in asphalt concrete pavements using an acoustic emission approach. *RILEM Bookseries* **13** (2016*)* 657-663, doi: 10.1007/978-94-024-0867-6_92.

[25] X. Li, M.O. Marasteanu, Investigation of Low Temperature Cracking in Asphalt Mixtures by Acoustic Emission, *Road Mater. Pavement* **7**(4) (2006) 491-512, doi: 10.1080/14680629.2006.9690048.

[26] Z.Q. Kang, Y. Yu, H. Wen, Damage Evolution of Rock and Acoustic Emission Study about Deep Diversion Tunnel in the Excavation Process, *Adv. Mat. Res.* **366** (2012) 243-246, doi: 10.4028/www.scientific.net/AMR.366.243.

[27] A. K. Maji, R. Sahu, Acoustic emissions from reinforced concrete, *Exp. Mech.* **34**(4) (1994) 379-388.

[28] A. Gu, Y. Luo, B. Xu, Continuous condition monitoring of reinforced concrete using an active diagnosis method, *Struct. Health. Monit.* **15**(1) (2016) 104-112, doi: 10.1177/1475921715624501.

[29] F. Rezaie, S.M. Farnam, Fracture mechanics analysis of pre-stressed concrete sleepers via investigating crack initiation length, *Eng. Fail. Anal.* **58** (2015) 267-280, doi: 10.1016/j.engfailanal.2015.09.007.

[30] A. Carpinteri, G. Lacidogna, F. Accornero, A.C. Mpalaskas, T.E. Matikas, D.G. Aggelis, Influence of damage in the acoustic emission parameters, *Cement Concrete Comp.* **44** (2013) 9-16, doi: 10.1016/j.cemconcomp.2013.08.001.

[31] Y. Farnam, M.R. Geiker, D. Bentz, J. Weiss, acoustic emission waveform characterization of crack origin and mode in fractured and ASR damaged concrete, *Cement Concrete Comp.* **60** (2015) 135-145, doi: 10.1016/j.cemcencomp.2015.04.008.

[32] H. Feng, W. Yi, Propagation characteristics of acoustic emission wave in reinforced concrete, *Results Phys.* **7** (2017) 3815-3819, doi: 10.1016/j.rinp.2017.09.060.

[33] W. Li, C. Xu, S.C.M. Ho, B. Wang, G. Song, Monitoring Concrete Deterioration Due to Reinforcement Corrosion by Integrating Acoustic Emission and FBG Strain Measurements, *Sensors* **17** (2017) 657-668, doi:10.3390/s17030657.

[34] D.J. Yoon, W.J. Weiss, S.P. Shah, Assessing damage in corroded reinforced concrete using acoustic emission, *J. Eng. Mech.* **126**(3) (2000) 273–283, doi: 10.1061/(ASCE)0733-9399(2000)126:3(273).

[35] Z. Li, F. Li, A. Zdunek, E. Landis, S.P. Shah, Application of acoustic emission technique to detection of rebar corrosion in concrete. *ACI Mater. J.* **95**(1) (1998) 68–81.

[36] S.C. Paul, S. Pirskawetz, G.P.A.G. van Zijl, W. Schmidt, Acoustic emission for characterising the crack propagation in strain-hardening cement-based composites (SHCC), *Cement Concrete Res.* **69** (2015) 19-24, doi: 10.1016/j.cemconres.2014.12.003.

[37] Sowjanya V, Sasibhushana Rao G and Sarvani A 2016 Investigation of Optimal Wavelet Techniques for De-noising of MRI Brain Abnormal Image *Procedia Comput. Sci.* **85** 669-675.

[38] Azzalini A, Farge M and Schenider K 2005 Nonlinear wavelet thresholding: A recursive method to determine the optimal denoising threshold *Appl. Comput. Harmon. Anal.* **18** 177-185.

[39] Zhang X, Feng N, Wang Y and Shen Y 2015 Acoustic emission detection of rail defect based on wavelet transform and Shannon entropy *J. Sound Vib.* **339** 419-432.

[40] CEMEX, Helping you to keep Britain's railways on track - Rail brochure (2014).

[41] British Standards Institute (BSI), European Standard BS EN13230 Railway applications. Track. Concrete sleepers and bearers, (2016) London UK.

[42] S. Kaewunruen, A.M. Remennikov, Nonlinear finite element modeling of railway prestressed concrete sleeper, Real Structures: Bridges and Tall Buildings - Proceedings of the 10th East Asia-Pacific Conference on Structural Engineering and Construction, EASEC Volume 4, The 10th East Asia-Pacific Conference on Structural Engineering and Construction, EASEC 2010; Bangkok; Thailand; 3 - 5 August 2006, pp. 323-328.

[43] https://uk.mathworks.com/help/stats/robustfit.html (Accessed on 21.02.2018.)

[44] https://www.physicalacoustics.com/wireless-systems/ (Accessed on 12.07.2018.)